J Nanostruct 14(4): 1296-1307, Autumn 2024

RESEARCH PAPER

Treatment of Biological-Wastewater from Cationic Dye Using Magnetic Nanocomposite Hydrogel: Characterization, Adsorption, and Application of Water Treatment

*Mohammed K. Kahlol [1], Aseel M. Aljeboree [2], Nadher D. Radia [3], Mohammed Abed Jawad [4], Ayad F. Alkaim [2]**

[1] *Department of Chemistry, Faculty of Science, Kufa University, AL-Najaf- Iraq*

[2] *Department of Chemistry, College of Sciences for Girls, University of Babylon, Hilla, Iraq*

[3] *Department of Chemistry, College of Education, University of Al-Qadisiyah, Al-Qadisiyah, Iraq*

[4] *Department of Pharmaceutics, Al-Nisour University College, Baghdad, Iraq*

ARTICLE INFO

Article History:
Received 22 June 2024
Accepted 28 September 2024
Published 01 October 2024

Keywords:
Crystal Violet
Dye Removal
Iron Nanoparticle
Isotherms
Nanocomposite Hydrogel

ABSTRACT

This study presents the development of a novel biocompatible polymer-based iron nanocomposite hydrogel. The synthesis involved grafting acrylic acid onto a cellulose backbone with simultaneous cross-linking. Methylenebisacrylamide was employed as a cross-linking agent, potassium persulfate was employed as a thermal initiator, and iron nanoparticles were incorporated as filling and reinforcing agents. A systematic optimization of factors affecting water absorption was conducted to achieve a superabsorbent with maximum swelling capacity. The efficacy of the synthesized iron hydrogel nanocomposite in the adsorption of crystal violet dye as a model cationic dye was investigated. The study examined the influence of various parameters on removal efficiency, including initial dye concentration, adsorbent dosage, contact time, and temperature. Additionally, thermodynamics, kinetics, and adsorption isotherms were analyzed. Results indicated that the adsorption method adheres to second model kinetics and the Langmuir adsorption isotherm. Based on experimental findings, the iron nanocomposite hydrogel demonstrates promising potential for environmental pollutant removal, particularly in eliminating toxic compounds from aqueous solutions.

How to cite this article
Kahlol M., Aljeboree A., Radia N., Jawad M., Alkaim A. Treatment of Biological-Wastewater from Cationic Dye Using Magnetic Nanocomposite Hydrogel: Characterization, Adsorption, and Application of Water Treatment. J Nanostruct, 2024; 14(4):1296-1307. DOI: 10.22052/JNS.2024.04.029

INTRODUCTION

Wastewater from textile and dyeing industries is considered one of the most hazardous effluents due to its content of chemicals, suspended solids, toxic compounds, and colorants (the primary pollutant detectable by the human eye). When discharged into rivers, dyes can degrade water quality and affect the photosynthetic function of aquatic plants by inhibiting sunlight penetration [1]. Furthermore, the presence of aromatic rings in the structure of organic dyes renders them carcinogenic and mutagenic, making them

* *Corresponding Author Email: alkaimayad@gmai.com*

biologically non-degradable [2]. Consequently, the removal of dyes from aqueous and biological samples is an essential and unavoidable task. Adsorption is one of the greatest usually applied method for dye elimination, exclusively for non-degradable dyes. This process involves two components: the adsorbent and the adsorbate. The adsorbent is the substance on which adsorption occurs, while the adsorbate is the species that is adsorbed onto the adsorbent [3]. Dye adsorption depends on the characteristics of the dye and the chemical surface of the adsorbent. Nanostructured adsorbents with high specific surface area and superior adsorption capacity generate less waste. Moreover, in addition to the high efficiency of adsorption processes, these materials can be regenerated and reused [4]. Nanoparticles can be employed to remove both organic and inorganic substances. However, their collection from solution surfaces requires prolonged centrifugation. Many materials at the nanoscale may potentially become toxic to the environment [5].

Hydrogels are soft in nature and usually have poor mechanical properties. The combination of Nano-gels with inorganic nanoparticles increases swelling and adsorption efficiency, thus improving mechanical and physical properties. Inorganic nanoparticles also increase the surface area of the surface. Iron oxide (Fe3O4) nanoparticles are of great importance in many applications, including adsorption, photocatalysis, and drug delivery, due to their small size, biocompatibility, and magnetic properties. Hydrogels can be combined with iron oxide as a surface coating. Biocompatibility due to their non-toxicity, high stability and increased activity of active groups on their surface.[6].

The functional groups present in the iron nanocomposite hydrogel were confirmed based on infrared spectroscopy. Then, the effect of various actors, including the contact time, weight of the hydrogel, temperature, and concentration of dye on removal efficiency, as well as thermodynamics, kinetics, and adsorption isotherm, were investigated. Additionally, due to the presence of iron on the surface and the existence of empty orbitals, the tendency for removing cationic substances increases. Furthermore, the separation of iron nanocomposite hydrogel is easily accomplished using a magnetic field. This separation method requires little energy and time. Based on the experimental results, iron nanocomposite hydrogel can be used to eliminate environmental pollutants, especially for removing toxic compounds from environmental solutions.

MATERIALS AND METHODS

Materials

We obtained potassium persulfate (KPS), methylene bisacrylamide (MBA), acrylic acid (AAc), crystal violet (CV), and ammonia from Merck, Germany. Cellulose, Iron (II) chloride tetrahydrate, and iron (III) chloride hexahydrate were purchased from Loba Chemie. All materials were used without purification, and double-distilled water was used for preparation and adsorption measurements.

Instrumental Analysis

For sample preparation and analysis, we used equipment such as a magnetic stirrer. A Shimadzu UV-visible 1650 PC spectrophotometer was utilized to measure concentrations. Infrared spectra of samples were obtained using a Jasco 4200 FT-IR spectrometer with potassium bromide pellets. The surface morphology of super absorbents was studied using scanning electron microscopy (SEM) images from a Philips XL30 model. Particle sizes were determined using transmission electron microscopy (TEM) images from a Zeiss TEM model. An AZ Company pH meter was utilized to study sample behavior at different pH levels, and a magnetic field was used to separate the adsorbent after the adsorption method.

Preparation of Iron Nanoparticle Synthesis

In a flask equipped with a nitrogen gas inlet and outlet, 1 g of $FeCl_2 \cdot 4H_2O$ and 2.6 g of $FeCl_3 \cdot 6H2O$ were dissolved in distilled water, and the reaction temperature was set to 70°C. 10 mL of ammonia was added dropwise to the mixture. The reaction continued for 1.5 h. The obtained product was placed in an oven at 50°C for 24 h to dry.

Preparation of Nanocomposite Hydrogel

In this step, we used KPS as an initiator and AAc as a monomer. MBA was used as a cross-linker, and cellulose was used as a substrate for iron nanocomposite synthesis. 1 g of cellulose was placed in a 250 mL beaker, and 70 mL of distilled water at 70°C was added. The beaker was placed in a 70°C water bath and mixed with a mechanical stirrer at 600 rpm for 10 minutes. After this time, 0.5 g of iron nanoparticles was added to the cellulose beaker and mixed for 20

min. MBA and AAc were then added. Finally, after homogenization, KPS was added. After 30 min, the beaker was removed from the bath to cool to room temperature. The iron nanocomposite hydrogel was dehydrated with ethanol and, after 24 h, filtered and placed in a vacuum oven to dry completely. The dried nanocomposite hydrogel was ground into powder and passed through a 60-mesh sieve to determine the swelling capacity.

Water Absorption Measurement

To measure the hydrogel nanocomposite's absorption, we used the tea bag method[7]. A sample of 0.2 g of nanocomposite hydrogel was placed in a fabric mesh similar to a tea bag (with small mesh holes) and immersed in 200 mL of water. After the nanocomposite hydrogel swelled in the mesh, the bag was hung to remove excess water. The swelling capacity was calculated using the following formula:

$$ES = \frac{W_2 - W_1}{W_1} \quad (1)$$

Where W_2 and W_1 are the weight of the swollen and the initial weight nanocomposite hydrogel respectively.

Adsorption Experiments

All adsorption experiments were conducted in a batch system. The standard solution of CV dye is prepared by dissolving 1g dye in 1000 ml of distilled water to obtain 1000 mg/L and it is used in the rest of the laboratory experiments .The maximum wavelength (λmax) for crystal violet dye was reported as 590 nm. Various environmental conditions and factors affecting the adsorption process were investigated, including initial dye concentration (10 to 100 mg/L), contact time (1 to 60 minutes), temperature (25 to 45°C), and adsorbent dosage (0.005 to 0.3 g). All experiments were performed in 50 mL of dye solution. In each experiment, the dye removal percentage (%) and adsorption capacity (mg/g) were calculated using the following equations:

$$\text{Removal } \% = \frac{C_0 - C_e}{C_0} \times 100 \quad (2)$$

$$q_e = \frac{C_0 - C_e}{W} \times V \quad (3)$$

RESULTS AND DISCUSSIONS

Synthesis Mechanism

Fig. 1 shows the prepere mechanism of the iron hydrogel nanocomposite based on polyacrylic acid. As an initiator, potassium persulfate (KPS) decomposes under heat and produces sulfate anion radicals. The sulfate anion radical attacks the

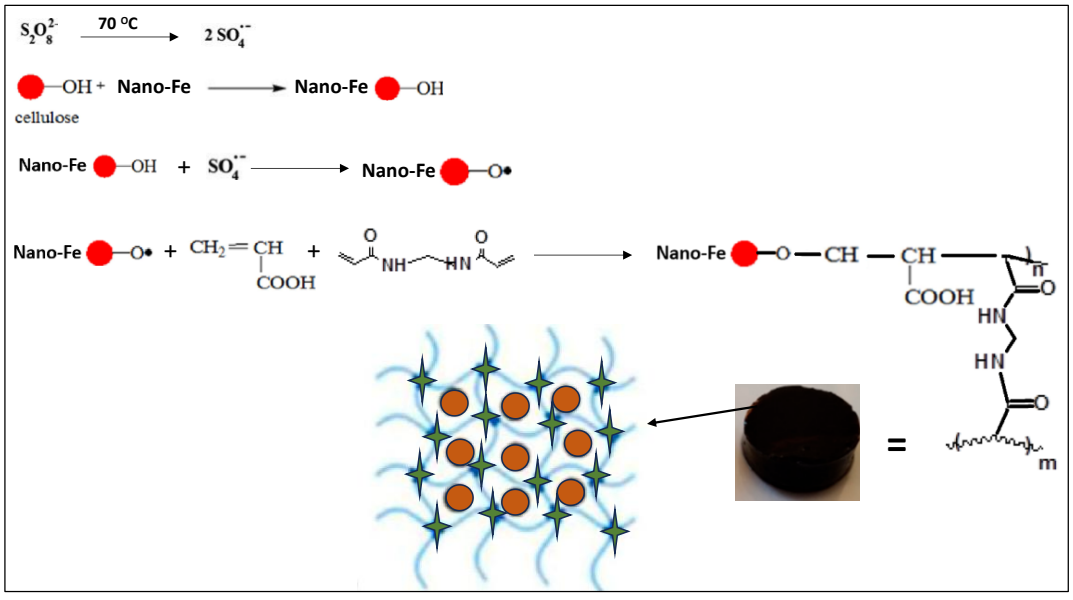

Fig. 1. A general mechanism for the synthesis of Iron Nanocomposite Hydrogel

hydrogen groups of anomeric carbon or hydroxyl present in the cellulose polysaccharide, breaking the C-H or O-H bond of the polysaccharide chain. The persulfate-saccharide redox system initiates a radical polymerization reaction, during which the acrylic acid (AAc) monomer is converted to polyacrylic acid (PAAc) and simultaneously binds to the polysaccharide chain. In the presence of the cross-linking agent methylene bisacrylamide (MBA), cross-links are formed in the structure of the cellulose-polyacrylic acid networked copolymer, creating the iron nanocomposite superabsorbent.

Optimization of Nanocomposite Hydrogel

To achieve the highest water absorption of the nanocomposite hydrogel, we optimized the most effective factors (monomer, cross-linker, and initiator) in its water absorption capacity.

As seen in Fig. 2-A, with increasing AAc concentration up to a certain limit, the water absorption of the nanocomposite hydrogel increases due to the increased rate of the polymerization reaction and the number of

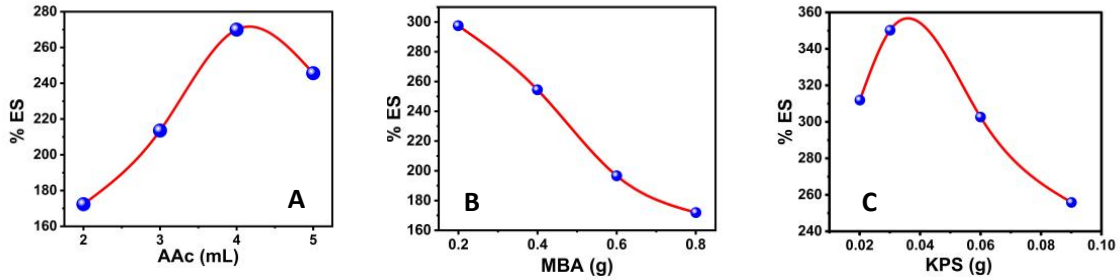

Fig. 2. (A) Effect amount of AAc, (B) MBA, and (C) APS on swelling capacity

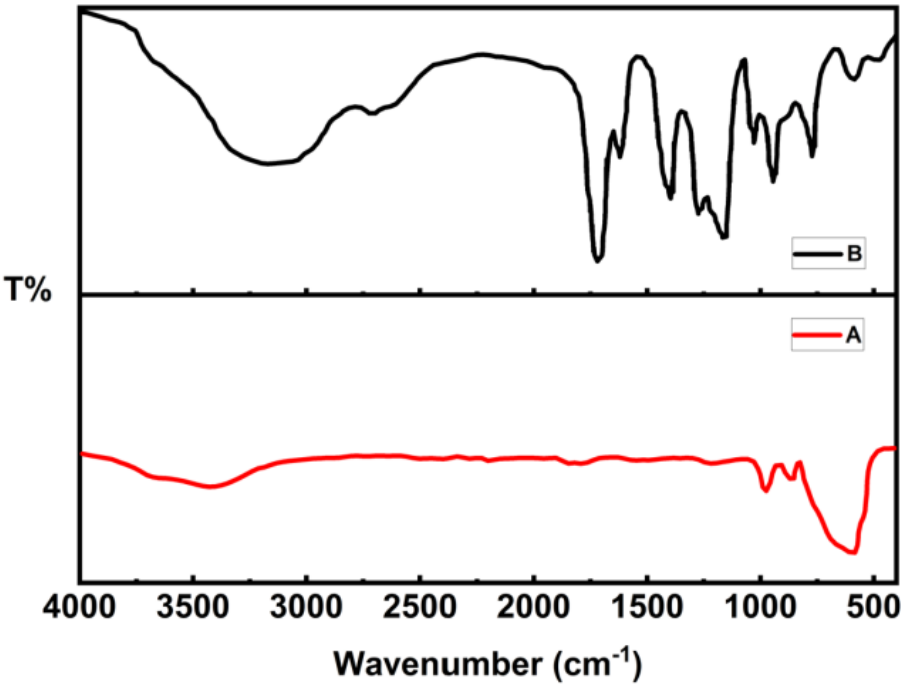

Fig. 3. FTIR spectrum of (A) iron nanoparticles and (B) iron nanocomposite hydrogel

hydrophilic functional groups of AAc along the hydrogel chain. Subsequently, the water absorption decreases, possibly due to the increased probability of AAc homopolymerization and slowing of free radical and AAc molecule movement[8].

Fig. 2-B shows the effect of changing MBA concentration on the water absorption of the nanocomposite hydrogel. With increasing cross-linker concentration, the degree of polymer chain cross-linking increases, and the available void spaces for water molecules decrease. This phenomenon causes a reduction in water absorption of the nanocomposite hydrogel at high MBA concentrations[9].

As observed in Fig. 2-C, with increasing KPS amount, the water absorption of the nanocomposite hydrogel decreases. The water absorption capacity initially increases due to the increased number of active sites (carboxylic acid) on the cellulose skeleton, making the nanocomposite hydrogel more hydrophilic. The decrease in absorption after the maximum value can be partly attributed to the increased cross-linking percentage through radical-radical chain encounters in radical termination reactions (self-cross-linking). Another important reason could be the degradation of cellulose chains in the presence of sulfate anion radicals[10].

The highest water absorption corresponds to

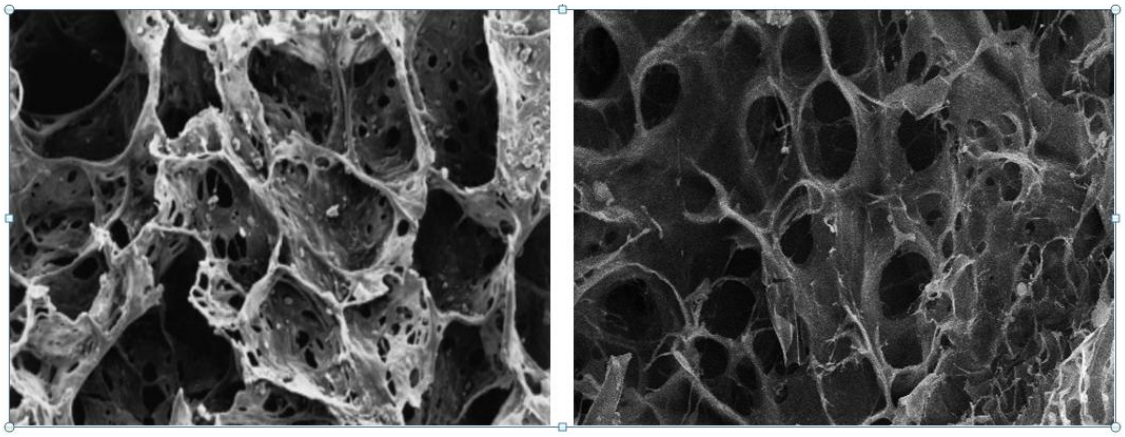

Fig. 4. SEM image of iron nanocomposite hydrogel

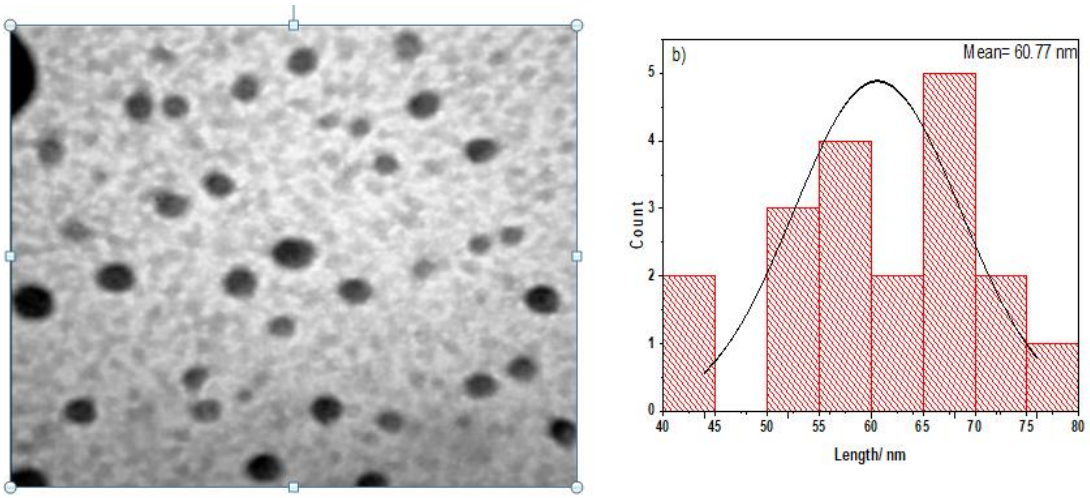

Fig. 5. TEM image of iron nanocomposite hydrogel a) Particle size distribution b).

the sample with 2 mL AAc, 0.02 g MBA, and 0.3 g KPS. All subsequent experiments and analyses were performed on this sample.

Adsorbent Characterization

FT-IR was utilized to identify and examine the present functional groups in the compounds. In the spectrum of iron nanoparticles, the peak at 588 cm^{-1} is characteristic of iron nanoparticles, and the peak at 3380 cm^{-1} could be due to stretching vibrations of water adsorbed on the nanoparticle surface. In the iron nanocomposite hydrogel spectrum, the peak at 1728 cm^{-1} can be attributed to the stretching vibrations of the carbonyl group (C=O), and the broad peak at 3270 cm^{-1} to the OH stretching vibration in polyacrylic acid and cellulose polysaccharide. The peak appearing in the 592 cm^{-1} region confirms that the iron nanoparticle is incorporated into the nanocomposite structure (Fig. 3).

The surface morphology of the hydrogel was examined through scanning electron microscopy (SEM) observations. As Fig. 4 shows, the synthesized iron nanocomposite hydrogel based on cellulose under optimal conditions contains pores in its structure. The porosity of hydrogel networks on its surface indicates the rate of hydrogel absorption[11, 12].

Fig. 5a shows the size of iron nanoparticles in the synthesized nanocomposite hydrogel using transmission electron microscopy (TEM). This image clearly shows the uniform distribution of iron nanoparticles on the hydrogel surface[13]. By measuring the nanoparticles in the TEM image and converting them to nanometers using the image scale, the average size of nanoparticles in the polymer network was found to be 9 to 11 nm and mean particle size is 60.77 nm as shown in Fig. 5b.

Adsorption Experiments

Effect of Adsorbent Dosage

Various amounts of adsorbent (0.005 to 0.3 g) were used to study the adsorbate dosage under ambient temperature conditions (25°C),pH solution, conc. of dye 50 mg/L, and an equilibrium time of 20 min. With a rise in the weight of the nanocomposite from 0.005 to 0.2 g, the removal % of crystal violet removal rises sharply, and with a further rise in adsorbent dosage, no significant change is observed. This increase is due to increased active sites and greater availability of adsorption sites. The optimal adsorbent dosage, according to Fig. 6, was determined to be 0.2 g .

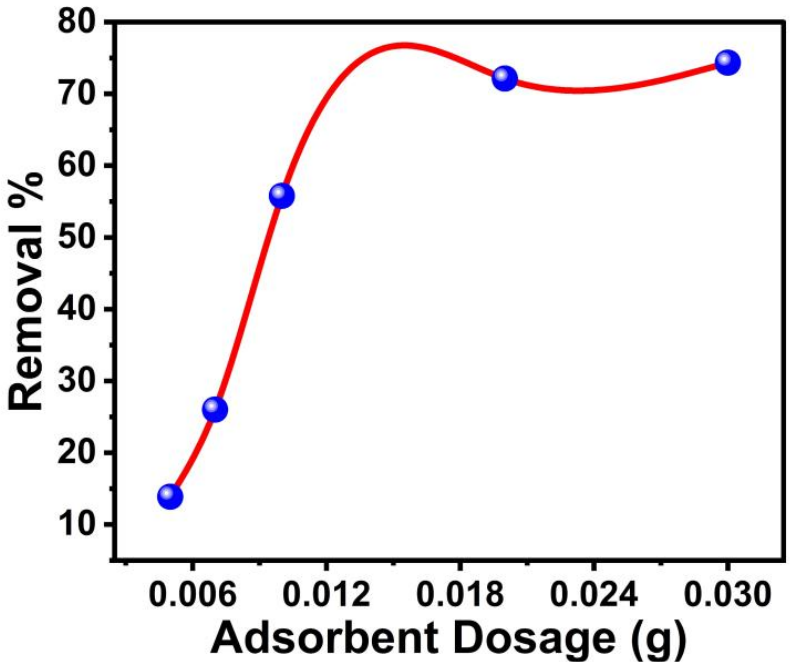

Fig. 6. Effect of adsorbent dosage on removal adsorption CV

Adsorption Kinetics Study

To study the kinetics adsorption of crystal violet, equilibrium times of 1 to 60 min were examined under ambient temperature conditions (25°C), the adsorbent dosage of 0.2 g, initial concentration of 50 mg/L, and pH=7. The experimental results indicated a suitable rate of CV adsorption on the adsorbent surface. As observed in Fig. 7, the adsorption rate is very high in the initial minutes and with time, the curve slope reaches an almost constant value. This is because, in the initial minutes, there are many empty cavities and pores, resulting in a high tendency for adsorption and extraction[6]. However, after 20 min, the empty cavities are filled, and the drug adsorption method reaches equilibrium, after which no significant change is observed with increasing time. Therefore, 20 min was selected as the optimal time.

Adsorption kinetics were studied using pseudo-first-order, pseudo-second-order, and Elovich equations by linear analysis method. The pseudo first order equation is expressed as follows [15]:

$$\log (q_e - q_t) = \log q_e - \frac{k_1}{2303} t \quad (4)$$

where qe and qt represent the adsorption efficiency at equilibrium and time t, respectively (mg/g). By plotting $\log(q_e - q_t)$ versus t, the values of q_e and k_1 can be obtained from the slope and intercept of the plot.

The pseudo-second-order kinetics is expressed as follows:[14, 15]

$$\frac{t}{q_t} = \frac{t}{q_e} + \frac{1}{k_2 q_e^2} \quad (5)$$

where k_2 is the rate constant of the pseudo-second-order equation (g/mg.min), q_e is the amount of adsorbed species at equilibrium (mg/g), and q_t is the amount of adsorbed species at time t. By plotting t/q_t versus t, the values of q_e and k_2 can be obtained.

The Elovich kinetics is expressed as follows:[16]

$$q_t = \frac{1}{\beta}\ln(\alpha\beta) + \frac{1}{\beta}\ln(t) \quad (6)$$

If the Elovich model is used, the relationship between q_t and ln(t) will be linear and completely

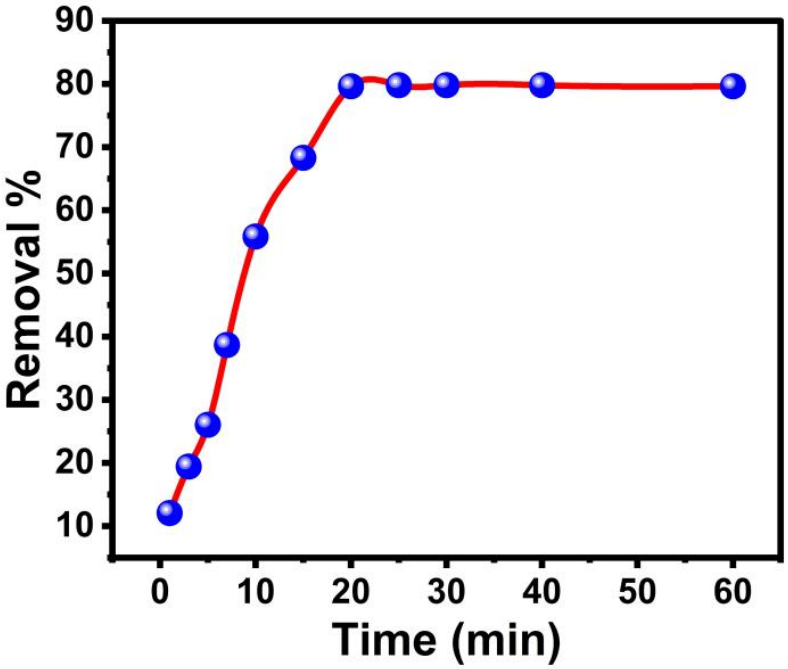

Fig. 7. Effect of contact time on removal adsorption CV

direct when plotting q_t versus ln(t).

According to Fig. 8, the pseudo-second-order kinetics better fits the experimental result due to the higher R2. Therefore, the adsorption of crystal violet follows the second model, and based on the theoretical assumptions, the nature of adsorption will be a chemical reaction and ion exchange.

Effect of Initial Dye Concentration and Adsorption Isotherm

To investigate the effect of initial concentration on CV adsorption, various concentrations (10 to 100 mg/L) were employed under ambient temperature conditions (25°C), with an adsorbent dosage of 0.2 g and pH 8. As shown in Fig. 9, the adsorption rate decreases with increasing dye concentration. The adsorption isotherm is of great importance and is used to describe the interaction between the adsorbate and the adsorbent. The equilibrium adsorption isotherm, based on a mathematical relationship (empirical or analytical), defines the amount of adsorbate adsorbed on the adsorbent (q_e in mg/g) per gram of adsorbent as a function of the equilibrium amount in solution (C_e in mg/L, the amount of non-adsorbed material) at a constant temperature[17].

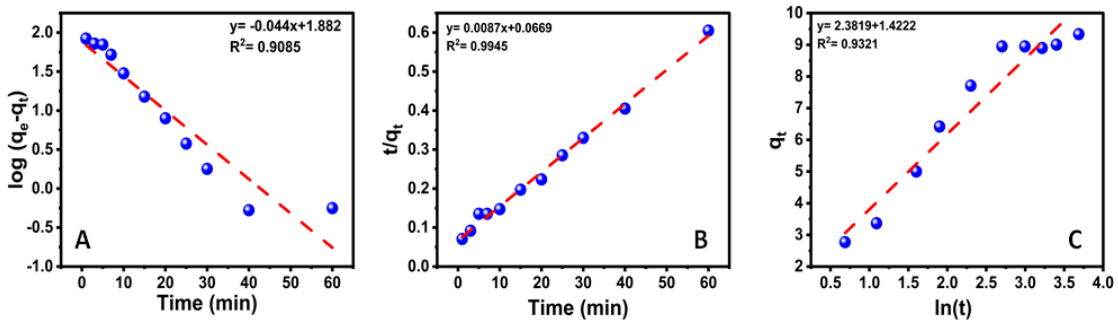

Fig. 8. Adsorption kinetics model (A) Pseudo-first-order, (B) Pseudo-second-order, (C) Elovich

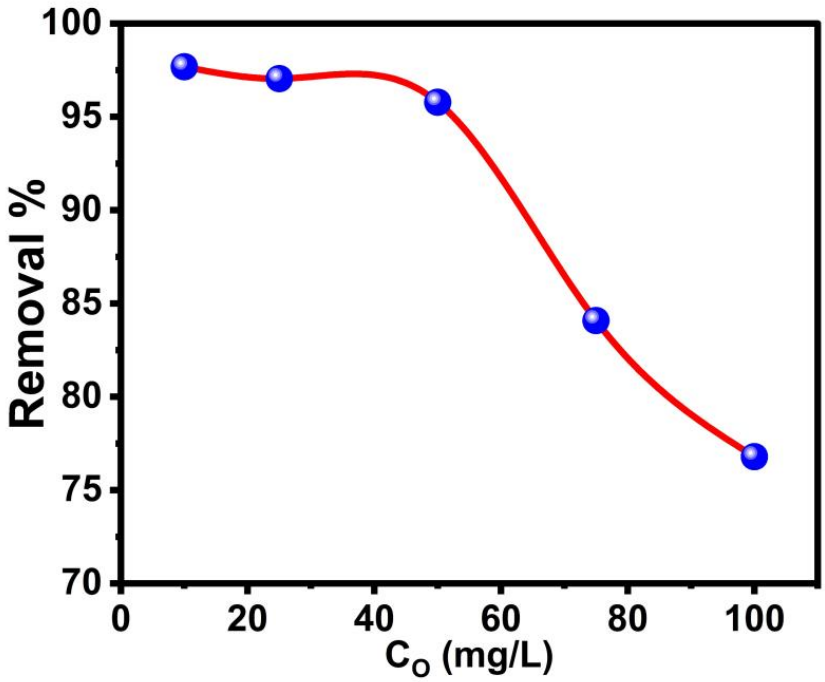

Fig. 9. Effect of initial concentration removal adsorption CV

We analyzed the adsorption isotherm results using two models: the Langmuir adsorption isotherm and the Freundlich adsorption isotherm. The Langmuir model is expressed as follows:

$$\frac{c_e}{q_e} = \frac{c_e}{q_m} + \frac{1}{k_L q_e} \quad (7)$$

Where q_e is the equilibrium adsorption efficiency (mg/g), C_e is the equilibrium dye concentration (mg/L), and q_m is the higher adsorption efficiency (mg/g). To examine the adherence of adsorption to this law, we plotted C_e/q_e versus C_e and calculated K_L and q_m from the y-intercept and slope.

The Freundlich isotherm is expressed as follows[18]:

$$\log q_e = \log k_f + \frac{1}{n} \log C_e \quad (8)$$

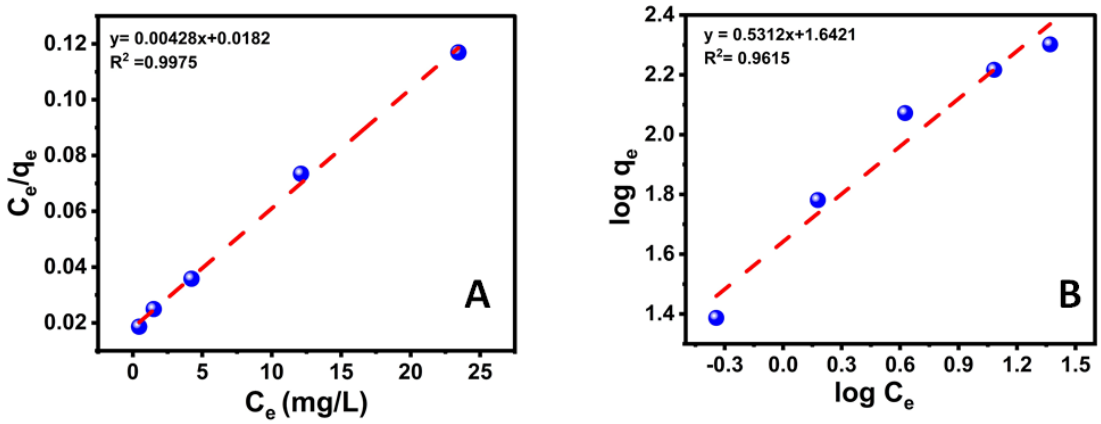

Fig. 10. Adsorption isotherm model: (A) Langmuir, and (B) Freundlich

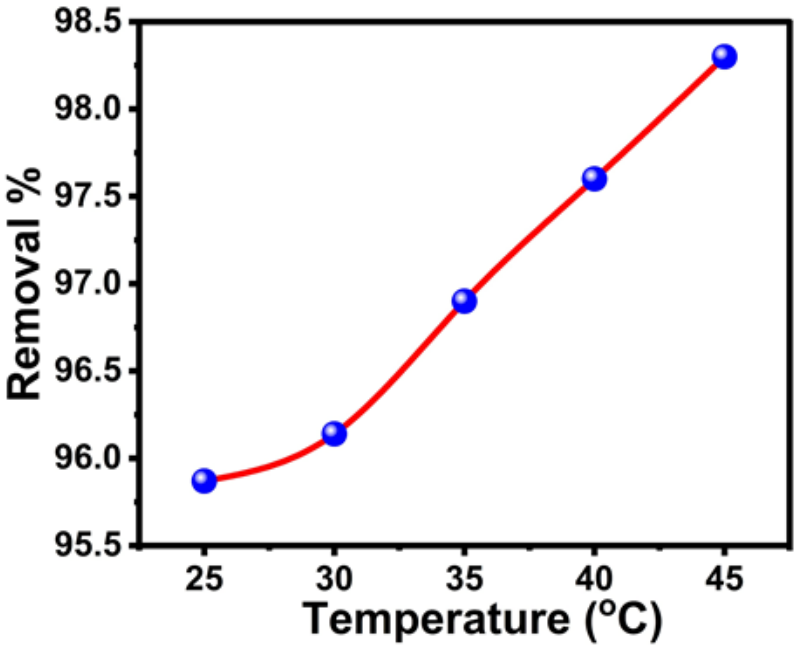

Fig. 11. Effect of temperature on removal adsorption CV

Where q_e is the equilibrium adsorption efficiency (mg/g), Ce is the equilibrium dye concentration (mg/L), and if and n are Freundlich constants, which we calculated from the y-intercept and slope by plotting log q_e versus log C_e.

According to Fig. 10, due to the higher correlation coefficient, the Langmuir adsorption isotherm shows a better fit with the experimental data. In accordance with the theory's assumptions, surface adsorption occurs as a single layer with equal energy and uniform sites [19, 20].

Effect of Temperature

Another significant parameter in adsorption studies is the investigation of the temperature effect. As shown in Fig. 11, with an increase in temperature from 15 to 45°C, the adsorption percentage has increased, which approximately corresponds to the swelling behavior of the iron nanocomposite hydrogel.

One of the important thermodynamic parameters is the Gibbs free energy, which is a thermodynamic quantity indicating the spontaneity of a reaction. A reaction is thermodynamically feasible when the change in Gibbs free energy is negative. The Gibbs free energy was obtained through equations (9) and (10). In these equations, ΔG is the change in Gibbs free energy. In equation (9), R is the gas constant, T is the temperature in Kelvin, and K is the equilibrium constant of the reaction.

$$\Delta G = -RT \ln K \quad (9)$$

$$\Delta G = \Delta H - T\Delta S \quad (10)$$

Eq. 10 encompasses two factors that influence the feasibility of reactions. The first factor is enthalpy (ΔH), which includes energy changes during the reaction, comprising kinetic and potential energy; provided that the pressure on the system remains constant during the reaction. This factor is expressed in KJ/mol. The second factor is entropy (system disorder) and is expressed in KJ/mol.K. To obtain the value of ΔG, K was calculated from Eq. 11.

$$K = \frac{q_e}{C_e} \quad (11)$$

In this equation, K is the equilibrium constant of the reaction with the unit ml/g, q_e is the

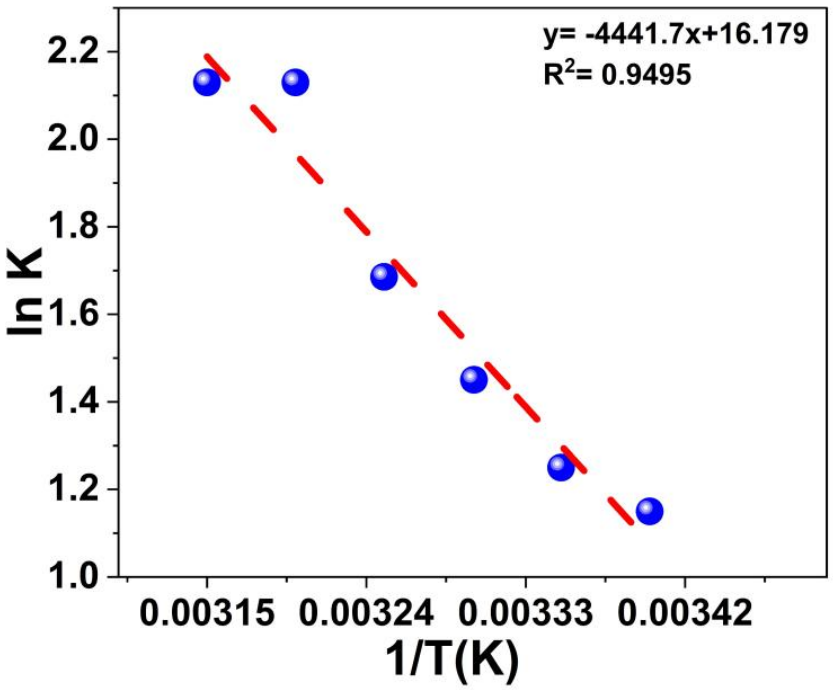

Fig. 12. Van't Hoff plot for the removal adsorption CV

Table 1. Calculated thermodynamic values at different temperatures

T(K)	ΔG^0(kJ/mol)	ΔH^0(kJ/mol)	ΔS^0(kJ/K.mol)
298	-3.097		
303	-3.654		
308	-4.316	23.60	134.51
313	-5.542		
318	-5.631		

Table 2. Removal of CV using several surfaces of nanocomposite.

hydrogel	pollutant	T (°C)	R%	Ref.
ZnO/(NaA-g-(Ac-coVBS)	CV	30	>80	[22]
(AMPSA-co-AA)	CV	30	80	[23]
(Nag-g-(PDMC-co-AC)	CV	20	91.3	[24]
Nag/Bn clay	CV	20	84.5	[25]
(Nag-co -AC)	CV	30	81.3	[26]
Nag-co-AM	CV	25	86.9	[27]
Nanocomposite	CV	25	93.1	In this study

equilibrium adsorption capacity in mg/g, and C_e is the drug concentration after adding the adsorbent at equilibrium. Then, the plot of lnK versus 1/T (Fig. 12) was drawn using the reaction equilibrium constant data and establishing the thermodynamic relationship between K and S (equation (12)). This plot has a slope equal to -ΔH/R and a y-intercept equal to ΔS/R. The values of ΔS and ΔH were obtained from the slope and y-intercept of the plot. The Gibbs free energy was calculated from the values of ΔS and ΔH. Due to the negative values obtained, the reaction is spontaneous [21]. These values are compiled in Table 1. In Table 2, the performance adsorption of the nanocomposite was compared with other nanocomposite on the high ability to eliminate CV dye.

$$\ln k = -\frac{\Delta H}{RT} + \frac{\Delta S}{R} \quad (12)$$

CONCLUSION

In this research, we synthesized an iron hydrogel nanocomposite based on poly (acrylic acid) grafted onto the bio-compatible polymer cellulose. Through skillful manipulation of structural factors, we obtained a superabsorbent with high adsorption capacity, suitable strength, and high swelling capacity. We then investigated the adsorption efficiency of crystal violet dye on the iron nanocomposite hydrogel. The experimental results indicated the high capacity of the adsorbent I n crystal violet adsorption. The morphological study of the nanocomposite hydrogel surface was conducted using SEM. In the SEM images, the pores of the hydrogel networks were evident, indicating the high water absorption capacity of the hydrogel. The size of iron nanoparticles and the uniform distribution of iron nanoparticles within the hydrogel network were determined using TEM. The maximum adsorption was determined under conditions of 35°C, an adsorbent amount of 0.02 g, pH 8, and a volume of 50 mL. The adsorption percentage under these optimal conditions was calculated to be 96.88%. Furthermore, the results showed that the adsorption process follows pseudo-second-order

kinetics and the Langmuir adsorption isotherm. Consequently, the iron nanocomposite hydrogel demonstrates high efficiency in the adsorption of cationic dyes.

CONFLICT OF INTEREST

The authors declare that there is no conflict of interests regarding the publication of this manuscript.

REFERENCES

1. Banerjee S, Sharma GC, Chattopadhyaya MC, Sharma YC. Kinetic and equilibrium modeling for the adsorptive removal of methylene blue from aqueous solutions on of activated fly ash (AFSH). Journal of Environmental Chemical Engineering. 2014;2(3):1870-1880.
2. Saeed T, Naeem A, Mahmood T, Ahmad Z, Farooq M, Farida, et al. Comparative study for removal of cationic dye from aqueous solutions by manganese oxide and manganese oxide composite. Int J Environ Sci Technol (Tehran). 2020;18(3):659-672.
3. De Gisi S, Lofrano G, Grassi M, Notarnicola M. Characteristics and adsorption capacities of low-cost sorbents for wastewater treatment: A review. Sustainable Materials and Technologies. 2016;9:10-40.
4. Burakov AE, Galunin EV, Burakova IV, Kucherova AE, Agarwal S, Tkachev AG, et al. Adsorption of heavy metals on conventional and nanostructured materials for wastewater treatment purposes: A review. Ecotoxicology and Environmental Safety. 2018;148:702-712.
5. Chkirida S, Zari N, Achour R, Hassoune H, Lachehab A, Qaiss Aek, et al. Highly synergic adsorption/photocatalytic efficiency of Alginate/Bentonite impregnated TiO_2 beads for wastewater treatment. J Photochem Photobiol A: Chem. 2021;412:113215.
6. Pourjavadi A, Nazari M, Hosseini SH. Synthesis of magnetic graphene oxide-containing nanocomposite hydrogels for adsorption of crystal violet from aqueous solution. RSC Advances. 2015;5(41):32263-32271.
7. Zhang K, Feng W, Jin C. Protocol efficiently measuring the swelling rate of hydrogels. MethodsX. 2019;7:100779-100779.
8. Czarnecka E, Nowaczyk J. Semi-Natural Superabsorbents Based on Starch-g-poly(acrylic acid): Modification, Synthesis and Application. Polymers. 2020;12(8):1794.
9. Deraman NF, Mohamed NR, Romli AZ. Swelling kinetics and characterization of novel superabsorbent polymer composite based on mung bean starch-filled poly(acrylic acid)-graft-waste polystyrene. International Journal of Plastics Technology. 2019;23(2):188-194.
10. Thakur S, Arotiba OA. Synthesis, swelling and adsorption studies of a pH-responsive sodium alginate–poly(acrylic acid) superabsorbent hydrogel. Polym Bull. 2018;75(10):4587-4606.
11. Malatji N, Makhado E, Ramohlola KE, Modibane KD, Maponya TC, Monama GR, et al. Synthesis and characterization of magnetic clay-based carboxymethyl cellulose-acrylic acid hydrogel nanocomposite for methylene blue dye removal from aqueous solution. Environmental Science and Pollution Research. 2020;27(35):44089-44105.
12. Mhammed Alzayd AA, Radia ND. A Novel Eco-friendly Bionanocomposite: Synthesis, Optimizing Grafting Factors, Characterization, Adsorption of Ofloxacin Hydrochloride, Reinforcement Elimination System to Pharmaceutical Contaminants. Journal of Polymers and the Environment. 2023;32(4):1821-1836.
13. Jiao Y, Wan C, Bao W, Gao H, Liang D, Li J. Facile hydrothermal synthesis of Fe_3O_4@cellulose aerogel nanocomposite and its application in Fenton-like degradation of Rhodamine B. Carbohydr Polym. 2018;189:371-378.
14. Chen Z, Ma W, Han M. Biosorption of nickel and copper onto treated alga (Undaria pinnatifida): Application of isotherm and kinetic models. J Hazard Mater. 2008;155(1-2):327-333.
15. Santos SCR, Boaventura RAR. Adsorption of cationic and anionic azo dyes on sepiolite clay: Equilibrium and kinetic studies in batch mode. Journal of Environmental Chemical Engineering. 2016;4(2):1473-1483.
16. Khaled A, Nemr AE, El-Sikaily A, Abdelwahab O. Removal of Direct N Blue-106 from artificial textile dye effluent using activated carbon from orange peel: Adsorption isotherm and kinetic studies. J Hazard Mater. 2009;165(1-3):100-110.
17. Wang J, Guo X. Adsorption isotherm models: Classification, physical meaning, application and solving method. Chemosphere. 2020;258:127279.
18. Allen SJ, McKay G, Porter JF. Adsorption isotherm models for basic dye adsorption by peat in single and binary component systems. Journal of Colloid and Interface Science. 2004;280(2):322-333.
19. Chemistry International CI. Adsorption of crystal violet dye onto olive leaves powder: Equilibrium and kinetic studies. Center for Open Science; 2021.
20. Radia ND, Aljeboree AM, Mhammed AAA. Enhanced removal of crystal violet from aqueous solution using carrageenan hydrogel nanocomposite/MWCNTs. Inorg Chem Commun. 2024;167:112803.
21. Aljeboree AM, Essa SM, Kadam ZM, Dawood FA, Falah D, Alkaim AF. Environmentally Friendly Activated Carbon Derived from Palm Leaf for the Removal of Toxic Reactive Green Dye. International Journal of Pharmaceutical Quality Assurance. 2023;14(01):12-15.
22. Aljeboree AM, Albdairi HK, Alkaim AF, Mahdi AB, Salman AW, A JM. Synthesis, characterization, and applicability of an acrylic acid-grafted sodium alginate- based Zinc oxide hydrogel nanocomposite for crystal violet dye removal. Research Square Platform LLC; 2022.
23. Mittal H, Al Alili A, Morajkar PP, Alhassan SM. Graphene oxide crosslinked hydrogel nanocomposites of xanthan gum for the adsorption of crystal violet dye. J Mol Liq. 2021;323:115034.
24. Zhao Y, Chen Y, Zhao J, Tong Z, Jin S. Preparation of SA-g-(PAA-co-PDMC) polyampholytic superabsorbent polymer and its application to the anionic dye adsorption removal from effluents. Sep Purif Technol. 2017;188:329-340.
25. Oladipo AA, Gazi M. Enhanced removal of crystal violet by low cost alginate/acid activated bentonite composite beads: Optimization and modelling using non-linear regression technique. Journal of Water Process Engineering. 2014;2:43-52.
26. Hameed KAA, Radia ND. Preparation and Characterization of Graphene Oxide (Sodium Alginate-g-polyacrylic Acid) Composite: Adsorption Kinetic of Dye Rose Bengal from Aqueous Solution. Neuroquantology. 2022;20(3):24-31.
27. Priya, Sharma AK, Kaith BS, Tanwar V, Bhatia JK, Sharma N, et al. RSM-CCD optimized sodium alginate/gelatin based ZnS-nanocomposite hydrogel for the effective removal of biebrich scarlet and crystal violet dyes. Int J Biol Macromol. 2019;129:214-226.